

High-pressure study on calcium azide (Ca(N$_{\bf 3}$)$_{\bf 2}$): Bending of azide ions stabilizes the structure

Xiaoxin Wu(武晓鑫), Yingjian Wang(王颖健), SiqiLi(李思琪), Juncheng Lv(吕俊呈), JingshuWang(王婧姝), Lihua Yang(杨丽华), Qi Zhang(张旗), Yanqing Liu(刘艳清), Junkai Zhang(张俊凯), and HongshengJia(贾洪声)

Citation: Chin. Phys. B, 2024, 33 (**5**): 056201. DOI: 10.1088/1674-1056/ad2b53
Journal homepage: http://cpb.iphy.ac.cn; http://iopscience.iop.org/cpb

What follows is a list of articles you may be interested in

Stability and melting behavior of boron phosphide under high pressure

Wenjia Liang(梁文嘉), Xiaojun Xiang(向晓君), Qian Li(李倩), Hao Liang(梁浩), and Fang Peng(彭放)
Chin. Phys. B, 2024, 33 (**4**): 046201. DOI: 10.1088/1674-1056/ad23d4

Pressure induced insulator to metal transition in quantum spin liquid candidate $NaYbS_2$

Yating Jia(贾雅婷), Chunsheng Gong(龚春生), Zhiwen Li(李芷文), Yixuan Liu(刘以轩), Jianfa Zhao(赵建发), Zhe Wang(王哲), Hechang Lei(雷和畅), Runze Yu(于润泽), and Changqing Jin(靳常青)
Chin. Phys. B, 2023, 32 (**9**): 096201. DOI: 10.1088/1674-1056/accff0

New MgO-H_2O compounds at extreme conditions

Lanci Guo(郭兰慈) and Jurong Zhang(张车荣)
Chin. Phys. B, 2023, 32 (**7**): 076201. DOI: 10.1088/1674-1056/ace035

Pressure-induced structural transition and low-temperature recovery of sodium pentazolate

Zitong Zhao(赵梓彤), Ran Liu(刘然), Linlin Guo(郭琳琳), Shuang Liu(刘爽), Minghong Sui(隋明宏), Bo Liu(刘波), Zhen Yao(姚震), Peng Wang(王鹏), and Bingbing Liu(刘冰冰)
Chin. Phys. B, 2023, 32 (**4**): 046202. DOI: 10.1088/1674-1056/acb917

In situ study of calcite-III dimorphism using dynamic diamond anvil cell

Xia Zhao(赵霞), Sheng-Hua Mei(梅升华), Zhi Zheng(郑直), Yue Gao(高悦), Jiang-Zhi Chen(陈姜智), Yue-Gao Liu(刘月高), Jian-Guo Sun(孙建国), Yan Li(李艳), and Jian-Hui Sun(孙建辉)
Chin. Phys. B, 2022, 31 (**9**): 096201. DOI: 10.1088/1674-1056/ac6157

High-pressure study on calcium azide ($Ca(N_3)_2$): Bending of azide ions stabilizes the structure

Xiaoxin Wu(武晓鑫)[1,2], Yingjian Wang(王颖健)[1,2], Siqi Li(李思琪)[1,2], Juncheng Lv(吕俊呈)[1,2], Jingshu Wang(王婧姝)[1,2], Lihua Yang(杨丽华)[1,2], Qi Zhang(张旗)[1,2], Yanqing Liu(刘艳清)[1,2], Junkai Zhang(张俊凯)[1,2,†], and Hongsheng Jia(贾洪声)[1,2,‡]

[1] *Key Laboratory of Functional Materials Physics and Chemistry (Ministry of Education), College of Physics, Jilin Normal University, Changchun* 130103, *China*

[2] *The Joint Laboratory of MXene Materials, Jilin Normal University & Jilin* 11 *Technology Co., Ltd., Changchun* 130103, *China*

(Received 18 December 2023; revised manuscript received 5 February 2024; accepted manuscript online 21 February 2024)

The high-pressure structure and elastic properties of calcium azide ($Ca(N_3)_2$) were investigated using *in-situ* high-pressure x-ray diffraction and Raman scattering up to 54 GPa and 19 GPa, respectively. The compressibility of $Ca(N_3)_2$ changed as the pressure increased, and no phase transition occurred within the pressure from ambient pressure up to 54 GPa. The measured zero-pressure bulk modulus of $Ca(N_3)_2$ is higher than that of other alkali metal azides, due to differences in the ionic character of their metal-azide bonds. Using CASTEP, all vibration modes of $Ca(N_3)_2$ were accurately identified in the vibrational spectrum at ambient pressure. In the high-pressure vibration study, several external modes (ext.) and internal bending modes (ν_2) of azide anions (N_3^-) softened up to ~ 7 GPa and then hardened beyond that pressure. This evidence is consistent with the variation observed in the F_E–f_E data analyzed from the XRD result, where the slope of the curve changes at 7.1 GPa. The main behaviors under pressure are the alternating compression, rotation, and bending of N_3^- ions. The bending behavior makes the structure of $Ca(N_3)_2$ more stable under pressure.

Keywords: high pressure, calcium azide, azide anions

PACS: 62.50.–p

DOI: 10.1088/1674-1056/ad2b53

1. Introduction

Inorganic azide was first synthesized by Curtius in the 1890s.[1] The azides have been found to be sensitive to heat, light, irradiation, shock, and so on.[2] They are widely used in industry as gas generators, photographic materials and pure nitrogen sources.[3] Several azides were observed to undergo structural phase transitions at pressures below 1 GPa during the 1970s.[4] These materials could also serve as theoretical models for studying fast reactions, structural stability,[5] lattice dynamics,[6,7] and electronic structure[8] of crystalline solids with complex chemical bonding. Recently, investigations into inorganic azides have become a popular research topic due to their potential for forming polymeric nitrogen networks than N_2.[9] With the development of the static high-pressure experimental technique, Eremets *et al.* transformed NaN_3 to a nonmolecular nitrogen state at 120 GPa.[10] This pressure is lower than that required to form nonmolecular nitrogen state using molecular nitrogen as a precursor, which is about 200 GPa and exhibits significant hysteresis.[11,12] In order to explore the better methods of forming polymeric nitrogen networks, a great deal of high-pressure experimental studies on monovalent azides AN_3 (A = Li,[13] Na,[14] K,[15] Ru,[16] Cs,[17] Ag,[18] NH_4[19,20]) have been conducted up to ~ 50 GPa in recent years due to the excellent properties of the azides. Most of these azides exhibit one or more phase transitions in the studied pressure regions.

Most high-pressure studies of the azides have focused on monovalent azides. Only a few researches have investigated the behavior of divalent azides under pressure.[21,22] These materials may serve as better precursors for the formation of polymeric nitrogen networks than monovalent azides because a mole of divalent azide contains twice as much nitrogen as a mole of monovalent azide. Based on this point, our interest was aroused by the alkaline-earth metal azides $B(N_3)_2$ (B = Mg, Ca, Sr, Ba).[23,24] As a typical series of divalent azides, alkaline-earth metal azides are characterized by their partial ionic nature and can be classified as ionic compound.[25] They are less energetic than all other inorganic azides, but still more energetic than alkali metal azides.[26,27] Accordingly, a detailed study of a certain alkaline-earth metal azide provides data for determining its structural stability, lattice dynamics, etc. Our previous study revealed that $Sr(N_3)_2$ transforms to an amorphous phase lower than 33.5 GPa.[21] In this paper, $Ca(N_3)_2$ is selected for studying. Krischner and Kelz determined the crystal structure, atomic fractional coordinates, and lattice parameters of $Ca(N_3)_2$.[28] They pointed out that the N_3^- ions in $Ca(N_3)_2$ are bent, which is different from all univalent azides. Olaf Reckeweg and Arndt Simon have listed the peak positions of the Raman and IR spectra,

†Corresponding author. E-mail: zjk8688@126.com
‡Corresponding author. E-mail: jiahs@jlnu.edu.cn

© 2024 Chinese Physical Society and IOP Publishing Ltd

which will serve as a contrast to our study.[29] Despite the extensive studies on alkali metal azides, further research is needed to supplement the behaviour of alkaline-earth metal azides under pressure.

In the present paper, the vibrational modes were assigned by theoretical modeling calculations of the vibrational spectrum using CASTEP code. Synchrotron x-ray diffraction and Raman scattering studies at pressures were performed to investigate structural stability and elastic properties of $Ca(N_3)_2$.

2. Experimental and computational method

2.1. Experimental method

The T301 steel sheets, which were utilized as gaskets, played a crucial role in sealing the sample chamber. A small hole was drilled in the center of the preloaded sheet. The holes in our experiments had an approximate diameter of 100 μm and a thickness of around 50 μm. To accurately measure the pressure within the chamber, the ruby fluorescence was employed.[30] In order to conduct high-pressure synchrotron x-ray studies and Raman studies under relatively hydrostatic pressure, a mixture consisting of methanol and ethanol with a volume ratio of 4:1 would serve as pressure-transmitting medium.

The high-pressure x-ray diffraction measurements were conducted at BSRF 4W2 (0.6199 Å). The MAR345 image plate detector was utilized to collect the diffraction patterns. The images were converted to 2θ versus intensity using FIT2D software. The structure was refined with Material Studio Software. High-pressure Raman scattering measurements were performed using a solid-state Nd: Vanadate laser (Coherent Inc.) with 532-nm excitation wavelength. The Acton SpectraPro 500i spectrometer, equipped with a liquid nitrogen-cooled CCD camera and a 1800-groove mm^{-1} grating, was used to record the Raman scattering spectra.

2.2. Computational method

All calculations performed in this paper are based on the first-principle plane-wave pseudo-potential density functional theory (DFT). CASTEP code was utilized for implement the theoretical modeling calculations. A norm-conserving pseudopotential is used with exchange and correlation effects described by the generalized-gradient-approximation (GGA) of Perdew–Burke–Ernzerhof (PBE).[31] In all calculations, convergence tests give a plane-wave energy cutoff E_{cutoff} as 770 eV and the electronic Brillouin zone (BZ) integration with the Monkhorst–Pack grid of spacing 0.02 $Å^{-1}$. The system was fully relaxed with respect to both internal atomic positions and cell size. The self-consistency cycle was considered converged when the total energy difference between two iterations was less than 10^{-6} eV/atom, and the geometry relaxation was stopped when the maximum atomic force in the system was less than 0.01 eV/atom. The vibrational frequencies of the optimized structure were then calculated.

3. Results and discussion

3.1. Powder x-ray diffraction at high pressures and equation of state

Figure 1 displays the crystal structure of $Ca(N_3)_2$ at ambient conditions. The 8*a*, 32*h*, and 16*e* are the Wyckoff positions of Ca, N(I), and N(II), respectively. One Ca^{2+} caion is encircled by eight N_3^- anions, and one N_3^- anion is located between four Ca^{2+} caions. $Ca(N_3)_2$ is an ionic compound, with N(I) separated from N(II) by a distance of 1.164 Å (Fig. 1(b)). It crystallizes in a layered structure similar to other alkali and alkaline-earth metal azides. The layers parallel to the (1 0 0) plane, as shown in Fig. 1.

The $Ca(N_3)_2$ powder was measured using high-pressure synchrotron x-ray diffraction up to 54 GPa at room temperature. Figure 2(a) presents the Rietveld refinement of the x-ray diffraction pattern at 0.7 GPa. All the observed diffraction peaks of $Ca(N_3)_2$ can be indexed into the orthorhombic structure and space group of *Fddd* (70) ($z = 8$), which is in accord with the JCPDS file No. 76-1141. The high-pressure XRD patterns are displayed in Fig. 2(b). The $Ca(N_3)_2$ maintains its *Fddd* structure up to 54 GPa because no new peak is observed throughout the compression process, which indicates that $Ca(N_3)_2$ has better phase stability than $Sr(N_3)_2$.

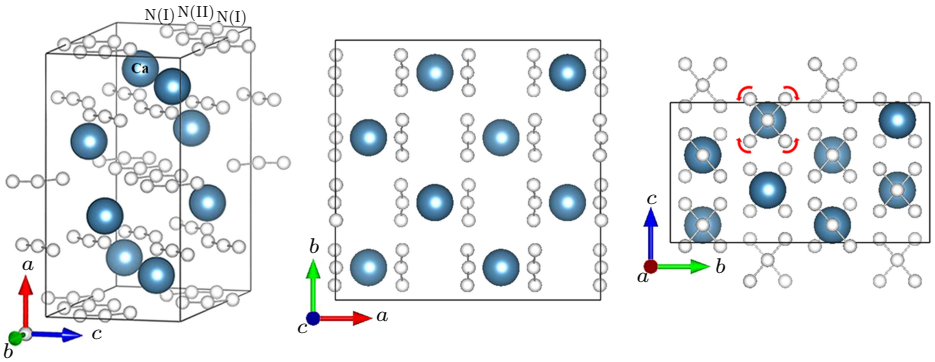


Fig. 1. Schematics of the crystal structure of $Ca(N_3)_2$ along *a*–*b*–*c* (a), *a*–*b* (b), and *b*–*c* (c) at ambient conditions. The red arrows denote the rotational directions of the N_3^- ions under pressure.

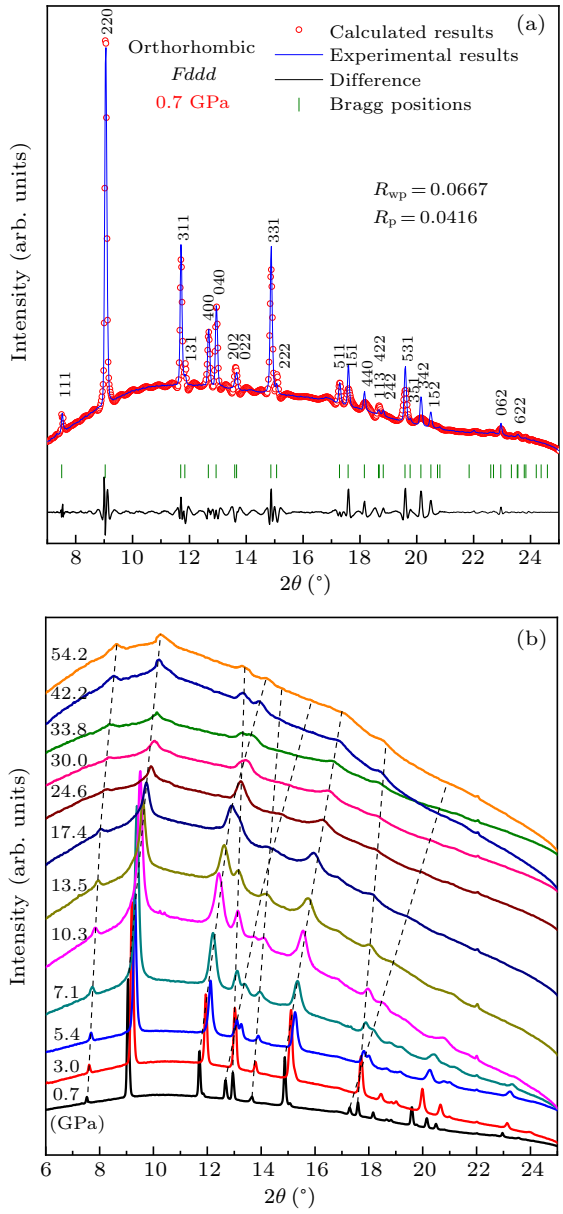


Fig. 2. (a) The Rietveld refinement of the XRD patterns of $Ca(N_3)_2$ taken at 0.7 GPa. The diffraction peaks are marked with bars and denoted with Miller indices. (b) High-pressure x-ray diffraction patterns of $Ca(N_3)_2$ at different pressures.

Figure 3(a) presents the variations of lattice parameters with pressure. The cell parameters a, b, and c exhibit an anisotropic compressibility up to 54 GPa, shrinking with rates of 79.74%, 96.86%, and 87.22% respectively in order of $a > c > b$. The most obvious lattice deformation occurs along the a axis, because the N_3^- ions lie in the orthorhombic bc planes oriented perpendicular to the a axis and the inter-layer direction is more compressive. In addition, the b axis is harder to be compressed than the c axis due to the rotational behavior of N_3^- ions under pressure. From the high-pressure study of $Sr(N_3)_2$ with the same structure of $Ca(N_3)_2$, it is known that the N^{3-} ions tend to rotate towards the ab planes under pressure, as shown by the red arrows in Fig. 1(c).[21] This rotation enhances the repulsion forces between N_3^- ions along the b axis and weakens them along the c axis, because it is more difficult to compress intramolecular force than intermolecular force. This phenomenon also occurs in other azides, where the rotational motion of N_3^- ions largely influences the compressibility, phase transition, and even hydrogen bonding energy of the crystal structure. As a result, the b axis exhibits the least compressibility and the deformation is concentrated within the basal ac plane. The anisotropy of compressibility results in a continuous decrease in the value of a/b, attaining $a = b$ at ~ 3 GPa (shown in the inset of Fig. 3(a)). The equation of two parameters can also be directly observed through the x-ray diffraction patterns (shown in the inset of Fig. 2(a)), where the diffraction peaks of (4 0 0) and (0 4 0) planes, as well as the (5 1 1) and (1 5 1) planes, merge into one peak at ~ 3 GPa respectively, and split with the increasing of pressure. The identical situation can also be observed in our previous high-pressure study on $Sr(N_3)_2$ (at 2.9 GPa), as the initial structures of $Ca(N_3)_2$and $Sr(N_3)_2$ are the same.[21] The separated variations of lattice parameters of a, b, and c are shown in Figs. 3(b)–3(d) to clearly exhibit the variations. The black arrows mark the points where there is a change in the slope of the curve. At ~ 7 GPa, there is a slight change in the slope of the curve for the a axis, while the b axis undergoes significant alterations. At ~ 30 GPa, all of the slope of the curve of a, b, and c axes change obviously. This is related to the transformations of the dominant compressive effects of the azide ions in $Ca(N_3)_2$ under pressure, which will be elaborated in the following.

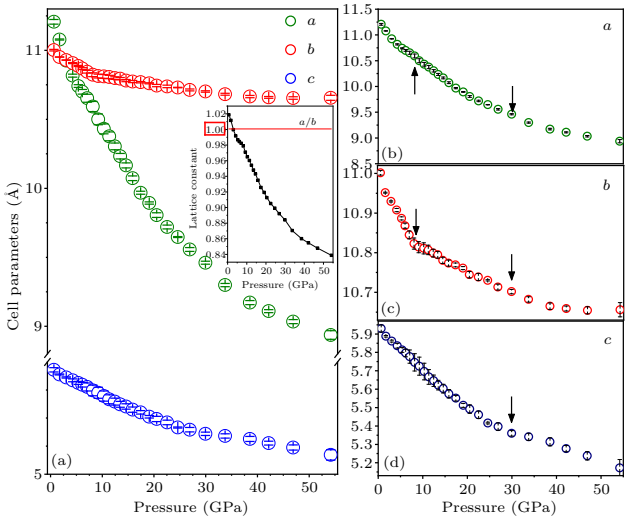


Fig. 3. (a) Pressure dependence of the cell volume (V) of $Ca(N_3)_2$. (b)–(d) Pressure dependence of the cell parameters (a, b, and c) of $Ca(N_3)_2$.

Figure 4(a) shows the pressure dependence of the cell volume of $Ca(N_3)_2$. During the compression, the unit cell of $Ca(N_3)_2$ is highly compressed with a volume of V (492.6 Å^3) at 54 GPa, that is just $\sim 66\%$ of the initial volume V_0 (745.6 Å^3). Fitting the pressure–volume data to the third-order Birch–Murnaghan (BM) equation of state (EOS) yields the bulk modulus value of $B_0 = 41.22 \pm 1.14$ GPa with $B_0' = 5.3 \pm 0.04$. The comparison of bulk modulus of several azides is summarized in Table 1. The bulk modulus of

alkaline-earth metal azides is larger than that of alkali metal azides, which can be ascribed to the different ionic characters. The alkaline-earth metal azides tend to have a more covalent nature compared to the alkali metal azides.[32] And the covalent character of alkaline-earth metal azides is similar to that of the heavy metal azides. Additionally, it can be concluded that the bulk modulus of alkaline-earth metal azides decreases slightly as atomic numbers increase. This rule is the same as that in the alkali metal azides (as shown in Table 1), which is ascribed to the different repulsive forces between the ions. As shown in Fig. 4(a), the black arrows also mark the points where there aare changes in the slopes of the curve as shown in Figs. 3(b)–3(d). The volume changes as the crystal parameters change. In order to give more insight of the variations, the F_E–f_E data calculated from the P–V data are shown in Fig. 4(b). The finite strain f_E is equal to $[(V_0/V)^{2/3}-1]/2$ and normalized pressure the F_E is equal to $P/(3f_E(1+2f_E)^{5/2})$.[33,34] Since the linear fit to the entire experimental data shows a positive slope (shown as red dashed line in Fig. 4(b)), a third-order BM EOS should adequately describe the data. The whole curve can be divided into three parts: a positive slope from 0–7.1 GPa; a negative slope from 7.1 GPa–30 GPa; and another positive slope from 30 GPa–54.2 GPa. The shape of the curve is influenced by the variational compressibilities of the b and c axes (the inflection points of the curves are indicated by arrows in Figs. 3(c) and 3(d)).

Table 1. Comparison of the bulk modulus B_0 of several azides.

		B_0 (GPa)	B_0'	Literature
Alkali metal azides	LiN_3	19.1		Ref. [18]
	α-NaN_3	17.3		Ref. [29]
	KN_3	18.6		Ref. [13]
	RbN_3	18.4		Ref. [15]
	α-CsN_3	18		Ref. [12]
Alkaline-earth Metal azides	$Sr(N_3)_2$	49.1 ± 1.1	2.5 ± 0.2	Ref. [27]
	$Ca(N_3)_2$	41.22 ± 1.14	5.3 ± 0.04	this work

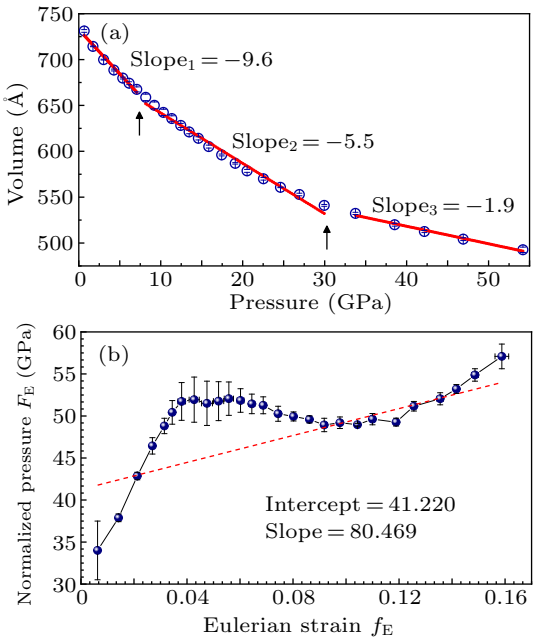


Fig. 4. (a) Pressure dependence of the cell volume of $Ca(N_3)_2$. The results are fitted to a third order Birch–Murnaghan equation. (b) The volume–pressure data of $Ca(N_3)_2$ displayed as a plot of the normalized pressure F_E against the Eulerian strain f_E. The error bar is the standard deviation of the mean.

3.2. Raman scattering at ambient and high pressures using calculated and experimental methods

The $Ca(N_3)_2$ was studied by use of *in-situ* Raman scattering. The primitive cell of $Ca(N_3)_2$ with orthorhombic structure and $Fddd$–D_{2h} space group contains 2 formula units, leaving 42 phonon modes. The group-theoretical treatment analysis predicts that at the zone center 39 optic modes of the orthorhombic structure. The irreducible representations are as follows:

$$\Gamma_{\text{optic}} = 4A_g^R + 4A_u + 6B_{1g}^R + 5B_{1u}^{IR} + 6B_{2g}^R + 5B_{2u}^{IR} + 5B_{3g}^R + 4B_{3u}^{IR}.$$

The A and B stand for nondegenerate vibrational modes. The g and u represent even and odd. The R and IR denote the modes are Raman-active and infrared-active, respectively.

Table 2. The mode frequencies of $Ca(N_3)_2$ in the experiment, calculation and reference at 0 GPa. The assignments are accomplished with calculations by CASTEP code.

Raman (cm^{-1}) Exp.	Raman (cm^{-1}) Exp.[25]	Calc.	Modes	Assignments[a]
68.6		68.8	$B_{3g}(1)$	$T(N_3^-)$
		140.2	$B_{3g}(2)$	$T(Ca^{2+})$
158.3	159	141.9	$A_g(1)$	$T(Ca^{2+})$
169.0		152.1	$B_{1g}(1)$	$T(Ca^{2+})$
		152.7	$B_{2g}(1)$	$R(N_3^-)$
174.8	175	166.2	$B_{2g}(2)$	$R(N_3^-)$
186.9	187	184.3	$B_{1g}(2)$	$R(N_3^-)$
		186.6	$A_g(2)$	$R(N_3^-)$
		198	$B_{1g}(3)$	$T(N_3^-)$
211.6	210	201.1	$B_{3g}(3)$	$T(N_3^-)$
228.9	229	217.1	$B_{2g}(3)$	$T(N_3^-)$
259.9	260	226.3	$B_{2g}(4)$	$R(N_3^-)$
		234.3	$B_{1g}(4)$	$R(N_3^-)$
636.5	637	607.6	$B_{3g}(4)$	ν_2
650.9	651	619.9	$A_g(3)$	ν_2
658.5	656	628.4	$B_{1g}(5)$	ν_2
		629.5	$B_{2g}(5)$	ν_2
1271.6	1271			$2\nu_2$
1283.1				$2\nu_2$
1300.2				$2\nu_2$
1312.3				$2\nu_2$
1356.2				$2\nu_2$ + ext.
1379.1	1379	1253.7	$A_g(4)$	ν_1
1383.3		1254.6	$B_{3g}(5)$	ν_1
2030	2031	1870.7	$B_{1g}(6)$	ν_3
2085.1		1917.8	$B_{2g}(6)$	ν_3

[a]R: libration, T: translation, ν_1: N=N=N symmetrical stretching, ν_2: N=N=N bending, ν_3: N=N=N asymmetrical stretching.

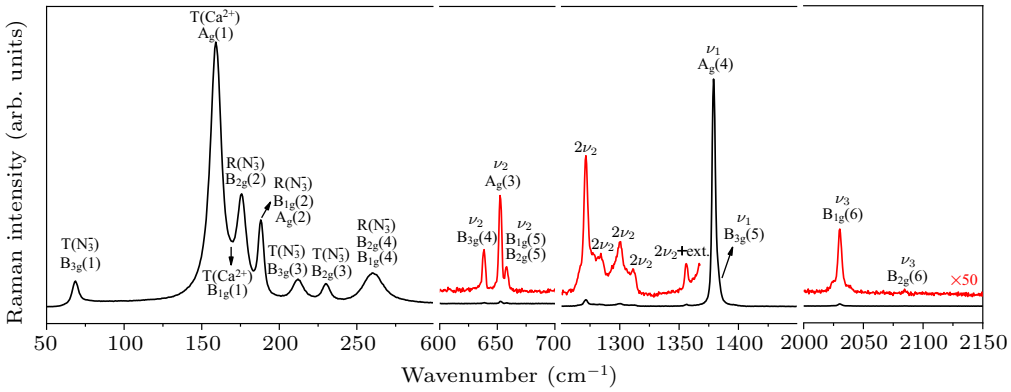


Fig. 5. Raman spectrum of $Ca(N_3)_2$ at ambient conditions. The red lines marked with ×50 represent the spectra was magnified by 50 times.

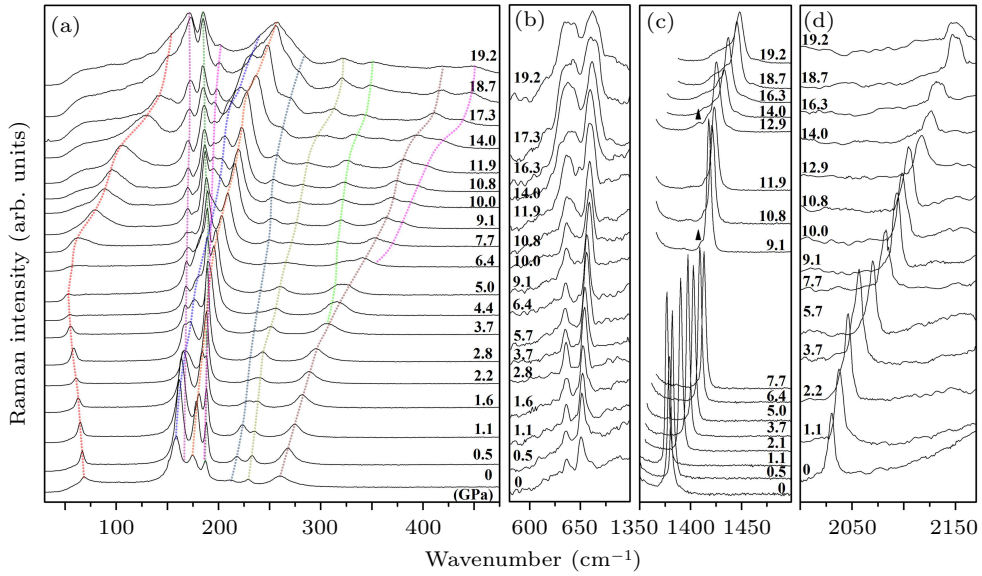


Fig. 6. Pressure-induced Raman spectra of lattice modes (a) together with the internal bending modes (b), symmetrical stretching modes (c), and asymmetrical stretching modes (d) of N_3^- up to ∼ 19.2 GPa.

Representative vibrational spectra of $Ca(N_3)_2$ were measured at ambient conditions within the range of 50 cm^{-1}–4000 cm^{-1}. The spectra can be roughly segmented into four parts: (i) the external (lattice) modes region between 50 cm^{-1}–450 cm^{-1}; (ii) the bending region between 600 cm^{-1}–700 cm^{-1}; (iii) the symmetric stretching region between 1300 cm^{-1}–1500 cm^{-1}; (iv) the asymmetric stretching region between 1900 cm^{-1}–2200 cm^{-1}. The frequencies along with the assignments are listed in Table 2. Several external modes are constructed with rotation–translation coupling, so the letters R and T in Table 2 indicate the prevailing types of motion. Certain differences exist due to the experimental conditions differ from the calculational conditions.

The Raman spectra of $Ca(N_3)_2$ at ambient conditions are presented in Fig. 5. There are 21 Raman-active modes out of the 39 optic modes. These spectra are in good agreement with the literature (listed in Table 2).[25] However, in external (lattice) modes region, one low-frequency mode at 68.6 cm^{-1} could not be observed in previous studies which may have been caused by the limited measuring range of the Raman scattering measurements. The mode at 68.6 cm^{-1}, together with the modes at 211.6 cm^{-1} and 228.9 cm^{-1}, represents the translations of the N_3^- ions. Three bands located at 174.8 cm^{-1}, 186.9 cm^{-1}, 259.9 cm^{-1} can be assigned to N_3^- librations. The band located at 158.3 cm^{-1} in the lattice modes frequency region represents translation of Ca^{2+} cation. These assignments were obtained through calculations using CASTEP code.

In fundamental intramolecular vibrations of N_3^- ions, symmetric stretching modes (ν_1), bending modes (ν_2), and asymmetric stretching modes (ν_3) are all allowed in Raman scattering, because of the nonlinear N_3^- ions in $Ca(N_3)_2$ exhibit polarization properties. The same goes for $Sr(N_3)_2$, $Ba(N_3)_2$, and $Pb(N_3)_2$, where N_3^- ions are also nonlinear and even asymmetric in $Ba(N_3)_2$ and $Pb(N_3)_2$. This phenomenon differs from the Raman vibrational activity of the symmetric and linear N_3^- ion in monovalent azide, where both bending modes (ν_2) and the asymmetric stretching modes (ν_3) are inactive. Among all internal vibrations of $Ca(N_3)_2$, the intensity of ν_1 modes apparently higher than that of other fundamental vibrations due to the symmetric and approximate linear shape of N_3^- ion. The strongest band, located at 1379.1 cm^{-1}, and the weaker high-frequency shoulder, located at 1383.3 cm^{-1}, are

identified as the in-phase ($A_g(4)$) and out-of-phase ($B_{3g}(5)$) symmetric stretching modes, respectively. The frequencies of the ν_1 modes are directly influenced by the length between the N–N bond. The N–N bond length of $Ca(N_3)_2$ is shorter than that in AN_3 (A = Li, Na, K, Ru, Cs, Ag, NH_4) and $B(N_3)_2$ (B = Sr, Ba), so the ν_1 frequency of $Ca(N_3)_2$ is the highest among these compounds. Due to the small bending angle of the N_3^- ion ($\sim 174.14°$), the bending modes (ν_2) at 640.5 cm^{-1}, 654.7 cm^{-1}, and 660.0 cm^{-1} as well as the asymmetric stretching modes (ν_3) at 2032.5 cm^{-1} and 2087.1 cm^{-1}, are very weak in the Raman spectra of $Ca(N_3)_2$. The weak bands at 1270 cm^{-1}–1330 cm^{-1} are assigned to the overtones of bending mode ($2\nu_2$), while the weak peak at 1356.2 cm^{-1} is attributed to a combination frequency of $2\nu_2$ and external translational modes based on analogy with the related metal azide.

The high-pressure Raman scattering on $Ca(N_3)_2$ was measured at the frequency range of 30 cm^{-1}–2200 cm^{-1} from ambient pressure up to 19.2 GPa. Representative spectra at evaluated pressures are presented in Fig. 6, while the pressure-dependent frequency shift is shown in Fig. 7. The patterns are divided into four plots because of the intensity of the peaks differs greatly.

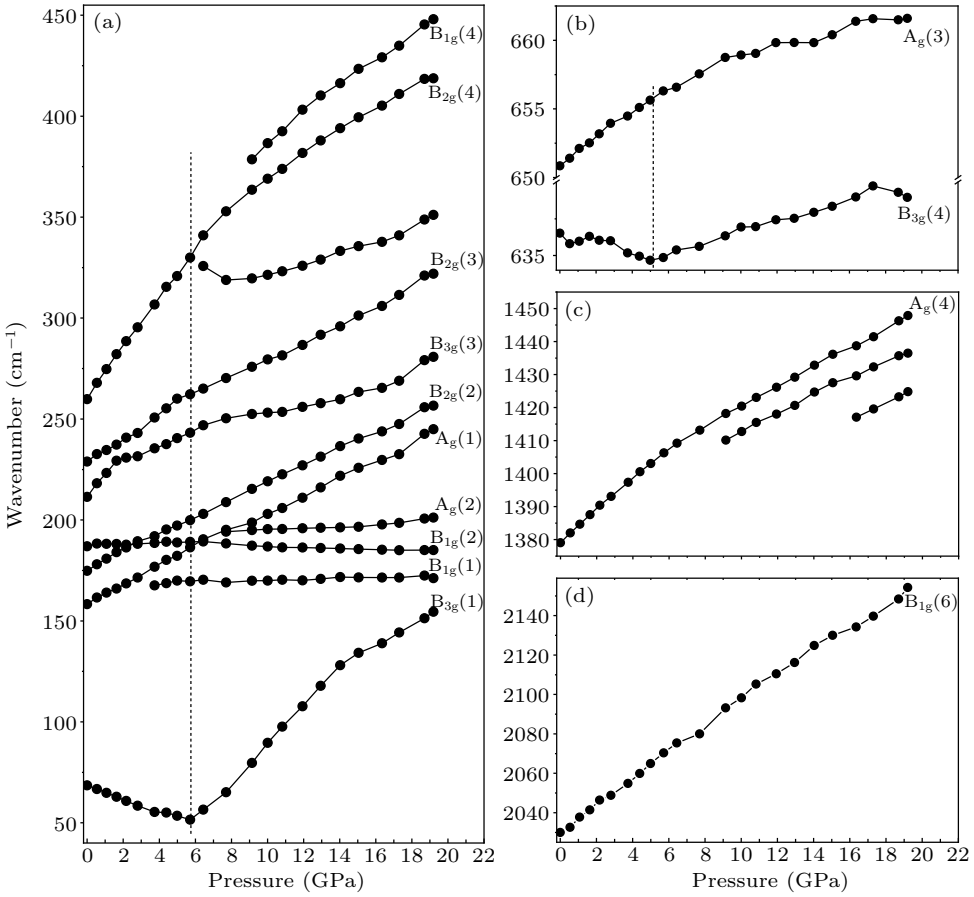


Fig. 7. Pressure dependence of frequencies of lattice modes (a) together with internal bending modes (ν_2) (b), symmetrical stretching modes (ν_1) (c), and asymmetrical stretching modes (ν_3) (d) of N_3^- up to $\sim$ 19.2 GPa.

As shown in Figs. 6 and 7, all modes, except the $B_{3g}(1)$, $B_{1g}(2)$, and $B_{3g}(4)$ modes, exhibit a monotonic shift to higher frequencies. The anisotropy of compressibilities results in different pressure coefficients. The $B_{3g}(1)$ and $B_{3g}(4)$ modes represent the translations and the in-phase bending vibrations of N_3^- ions along the c axis. With increased pressure up to $\sim$ 6 GPa, the N_3^- ions rotate towards the ab plane, which lengthens the distance between the adjacent N_3^- ions in the bc plane. Therefore the $B_{3g}(1)$ and $B_{3g}(4)$ modes soften from ambient pressure to $\sim$ 6 GPa. The result is in accord with our x-ray data. The softening of both translation and bending modes has been observed in a few systems with a layer structure, such as the compounds that exhibit the zircon-to-scheelite or zircon-to-monazite transition.[35]

It is worth noting that several changes occur at $\sim$ 6 GPa: the $B_{3g}(1)$ mode hardens from $\sim$ 6 GPa to higher pressure; the $B_{1g}(2)$ mode increases very slightly with pressure up to $\sim$ 6 GPa and then softens under subsequent compression; the mode at $\sim$ 325 cm^{-1} splits to the $B_{2g}(4)$ and $B_{1g}(4)$ modes. These changes are not induced by a structural phase transition, as evidenced by the x-ray results which show no new diffraction peak appearing at $\sim$ 6 GPa. However, they do coincide with the change in compressibility of the b axis at $\sim$ 7.1 GPa (Fig. 3(c)). From ambient pressure to about 7 GPa, the rota-

tion of the azide is the dominant behavior of the crystal compression, and the repulsion between the molecules of the azide is also increasing with the increase of the pressure. When it reaches about 7 GPa, the intermolecular repulsion of the azide ions reaches a certain degree. In order to ensure the stability of the lattice, the intramolecular bending of the azide ions have to be carried out to offset the intermolecular repulsion. At this time, the bending of the azide root occupies the dominant behavior of the crystal compression property. The bending behavior increases the freedom of N_3^- ions and makes the structure more stable under pressure. As the pressure continues to improve, the intermolecular repulsion and intramolecular bending of azide become stronger. When the pressure reaches about 30 GPa, the resistance to compression dominated by the bending of azide reaches a certain extent. In order to maintain the stability of the structure, the compression between the nitrogen atoms in the azide ions dominates the behavior of the crystal compression property.

4. Conclusion

The structural and elastic properties of calcium azide ($Ca(N_3)_2$) were investigated from ambient pressure up to 54 GPa, and no phase transition is observed within the pressure ranges achieved in this study. The compressibility properties of $Ca(N_3)_2$ are obviously influences by the orientation, rotation, and bending of N_3^-. The zero-pressure bulk modulus is higher than that of alkali metal azides, which can be ascribed to the different ionic character in the metal-azide bond. The vibrational spectra of $Ca(N_3)_2$ at ambient pressure have also been calculated using CASTEP to determine the assignments of all vibration modes. In the high-pressure vibration studies, several external modes and internal bending modes (ν_2) of N_3^- ions soften from ambient pressure to ~ 7 GPa and then reverse from ~ 7 GPa to higher pressure. The evidence is consistent with the change in the F_E–f_E data of the XRD result, where the curve shows a turning point at 7.1 GPa. The main behaviors under pressure are the alternating compression, rotation, and bending of N_3^- ions, which are responsible for the changes. The bending behavior of N_3^- ions contributes to the increased stability of the $Ca(N_3)_2$ structure under pressure.

Acknowledgements

The synchrotron x-ray diffraction measurements are technically supported by Beijing Synchrotron Radiation Facility (BSRF). Project supported financially by the Program for the Development of Science and Technology of Jilin Province, China (Grant Nos. YDZJ202301ZYTS382, YDZJ202201ZYTS316, and 20230101285JC), the National Natural Science Foundation of China (Grant No. 11904128), the Program for Science and Technology of Education Department of Jilin Province, China (Grant Nos. JJKH20220438KJ and JJKH20220423KJ), and the Program for the Jilin Provincial Development and Reform Commission Project (Grant No. 2022C040-6).

References

[1] Curtius T 1890 *Berichte der deutschen chemischen Gesellschaft* **23** 3023
[2] Evans B L, Yoffe A D and Gray P 1959 *Chem. Rev.* **59** 515
[3] Gray P 1963 *Quarterly Reviews, Chemical Society* **17** 441
[4] Ti S S, Kettle S F A and Ra 1977 *Journal of Raman Spectroscopy* **6** 5
[5] Evans B L and Yoffe A D 1957 *Proceedings of the Royal Society of London. Series A, Mathematical and Physical Sciences* **238** 568
[6] Rao K R 1970 *J. Chem. Phys.* **53** 4661
[7] Rafizadeh H A, Yip S and Prask H 1972 *J. Chem. Phys.* **56** 5377
[8] Younk E H and Kunz A B 1997 *Int. J. Quantum Chem.* **63** 615
[9] Badgujar D M, Talawar M B, Asthana S N and Mahulikar P P 2008 *Journal of Hazardous Materials* **151** 289
[10] Eremets M I, Popov M Y, Trojan I A, Denisov V N, Boehler R and Hemley R J 2004 *J. Chem. Phys.* **120** 10618
[11] Eremets M I, Hemley R J, Mao H K and Gregoryanz E 2001 *Nature* **411** 170
[12] Goncharov A F, Gregoryanz E, Mao H K, Liu Z and Hemley R J 2000 *Phys. Rev. Lett.* **85** 1262
[13] Medvedev S A, Trojan I A, Eremets M I, Palasyuk T, Klapötke T M and Evers J 2009 *J. Phys.: Condens. Matter* **21** 195404
[14] Zhu H, Zhang F, Ji C, Hou D, Wu J, Hannon T and Ma Y 2013 *J. Appl. Phys.* **113** 033511
[15] Ji C, Zheng R, Hou D, Zhu H, Wu J, Chyu M C and Ma Y 2012 *J. Appl. Phys.* **111** 112613
[16] Li D, Wu X, Jiang J, Zhang J, Cui Q, Zhu H and Wang X 2014 *Appl. Phys. Lett.* **105** 071903
[17] Hou D, Zhang F, Ji C, Hannon T, Zhu H, Wu J and Ma Y 2011 *Phys. Rev. B* **84** 064127
[18] Hou D, Zhang F, Ji C, Hannon T, Zhu H, Wu J, Levitas V I and Ma Y 2011 *J. Appl. Phys.* **110** 23524
[19] Wu X, Cui H, Zhang J, Cong R, Zhu H and Cui Q 2013 *Appl. Phys. Lett.* **102** 121902
[20] Wu X, Ma F, Ma C, Cui H, Liu Z, Zhu H, Wang X and Cui Q 2014 *J. Chem. Phys.* **141** 024703
[21] Zhu H, Han X, Zhu P, Wu X, Chen Y, Li M, Li X and Cui Q 2016 *J. Phys. Chem. C* **120** 12423
[22] Dong F, Cheng X and Ge S 2007 *J. Theor. Comput. Chem.* **06** 487
[23] Garner W E and Maggs J 1939 *Proceedings of the Royal Society A* **172** 299
[24] Deb S K 1963 *Transactions of the Faraday Society* **59** 1423
[25] Zhu W, Xu X and Xiao H 2007 *J. Phys. Chem. Solids* **68** 1762
[26] Zhu W and Xiao H 2010 *Structural Chemistry* **21** 657
[27] Zhu W, Xiao J and Xiao H 2006 *J. Phys. Chem. B* **110** 9856
[28] Krischner H and Kelz G 1982 *Zeitschrift für anorganische und allgemeine Chemie* **494** 203
[29] Reckeweg O and Simon A 2003 *Zeitschrift für Naturforschung B* **58** 1097
[30] Mao H K, Xu J and Bell P M 1986 *Journal of Geophysical Research: Solid Earth* **91** 4673
[31] Perdew J P, Burke K and Ernzerhof M 1996 *Phys. Rev. Lett.* **77** 3865
[32] Mauer F A, Hubbard C R and Hahn T 1973 *J. Chem. Phys.* **59** 3770
[33] Angel R J 2000 *Reviews in Mineralogy and Geochemistry* **41** 35
[34] Gomis O, Santamaría-Pérez D, Vilaplana R, Luna R, Sans J A, Manjón F J, Errandonea D, Pérez-González E, Rodríguez-Hernández P, Muñoz A, Tiginyanu I M and Ursaki V V 2014 *J. Alloys Compd.* **583** 70
[35] Panchal V, López-Moreno S, Santamaría-Pérez D, Errandonea D, Manjón F J, Rodríguez-Hernandez P, Muñoz A, Achary S N and Tyagi A K 2011 *Phys. Rev. B* **84** 024111